Molecular Pharmacology Fast Forward. Published on January 14, 2016 as DOI: 10.1124/mol.115.102533
This article has not been copyedited and formatted. The final version may differ from this version.

Binding to and inhibition of insulin-regulated aminopeptidase (IRAP) by macrocyclic disulfides enhances spine density

Shanti Diwakarla, Erik Nylander, Alfhild Grönbladh, Sudarsana Reddy Vanga, Yasmin Shamsudin Khan, Hugo Gutiérrez-de-Terán, Leelee Ng, Vi Pham, Jonas Sävmarker, Thomas Lundbäck, Annika Jenmalm-Jensen, Hanna Andersson, Karin Engen, Ulrika Rosenström, Mats Larhed, Johan Åqvist, Siew Yeen Chai, Mathias Hallberg

Beijer Laboratory, Department of Pharmaceutical Biosciences, Division of Biological Research on Drug Dependence (S.D., E.N., A.G., M.H.), Department of Cell and Molecular Biology (S.R.V., Y.S.K., H.G.T., J.A.), Beijer Laboratory, Department of Medicinal Chemistry (J.S.), Department of Medicinal Chemistry (H.A., K.E., U.R.), Science for Life Laboratory, Department of Medicinal Chemistry (M.L.), BMC, Uppsala University, Uppsala, Sweden; Chemical Biology Consortium Sweden, Science for Life Laboratory, Division of Translational Medicine and Chemical Biology, Department of Medicinal Biochemistry and Biophysics (T.L., A.J.), Karolinska Institute, Sweden; and Biomedicine Discovery Institute, Department of Physiology (L.N., V.P., S.Y.C.), Monash University, Melbourne, Australia

Molecular Pharmacology Fast Forward. Published on January 14, 2016 as DOI: 10.1124/mol.115.102533
This article has not been copyedited and formatted. The final version may differ from this version.

Running Title: Macrocyclic insulin-regulated aminopeptidase inhibitors

Corresponding Author:

A/Prof. Mathias Hallberg

Beijer Laboratory, Department of Pharmaceutical Biosciences, Division of Biological Research on Drug Dependence, BMC, Uppsala University, P.O. Box 591, SE-751 24, Uppsala, Sweden

Tel: +46 18 471 4141

Fax: +46 18 471 4253

Email: mathias.hallberg@farmbio.uu.se

Number of text pages: 38

Number of Tables: 1

Number of Figures: 8

Number of references: 96

Number of words:

Abstract = 248

Introduction = 684

Discussion = 1334

List of abbreviations: Ang IV, angiotensin IV; Ang IV-gt, Ang IV complex with the inverse γ-turn conformation; ANOVA, one-way analysis of variance; AP-N, aminopeptidase N; BDNF, brain derived neurotrophic factor; DAPI, 4',6-diamidino-2-phenylindole, dihydrochloride; DIV, days in vitro; ΔG_{bind}, binding free energies; IRAP, insulin-regulated aminopeptidase; LIE, linear interaction energy; LTA4H, leukotriene A4 hydrolase; LTP, long-term potentiation; MD, molecular dynamics; PBS, phosphate buffered saline; PDB, protein data bank; vGLUT1, vesicular glutamate transporter 1

Molecular Pharmacology Fast Forward. Published on January 14, 2016 as DOI: 10.1124/mol.115.102533
This article has not been copyedited and formatted. The final version may differ from this version.

Abstract

Angiotensin IV (Ang IV) and related peptide analogues, as well as non-peptide inhibitors of insulin-regulated aminopeptidase (IRAP), have previously been shown to enhance memory and cognition in animal models. Furthermore, the endogenous IRAP substrates oxytocin and vasopressin are known to facilitate learning and memory. In this study, the two recently synthesized 13-membered macrocyclic competitive IRAP inhibitors HA08 and HA09, which were designed to mimic the N-terminal of oxytocin and vasopressin, were assessed and compared based on their ability to bind to the IRAP active site, and alter dendritic spine density in rat hippocampal primary cultures. The binding modes of the IRAP inhibitors HA08, HA09 and of Ang IV in either the extended or γ-turn conformation at the C-terminal to human IRAP were predicted by docking and molecular dynamics (MD) simulations. The binding free energies calculated with the linear interaction energy (LIE) method, which are in excellent agreement with experimental data and simulations, have been used to explain the differences in activities of the IRAP inhibitors, both of which are structurally very similar, but differ only with regard to one stereogenic center. In addition, we show that HA08, which is 100-fold more potent than the epimer HA09, can enhance dendritic spine number and alter morphology, a process associated with memory facilitation. Therefore, HA08, one of the most potent IRAP inhibitors known today, may serve as a suitable starting point for medicinal chemistry programs aided by MD simulations aimed at discovering more drug-like cognitive enhancers acting via augmenting synaptic plasticity.

Molecular Pharmacology Fast Forward. Published on January 14, 2016 as DOI: 10.1124/mol.115.102533
This article has not been copyedited and formatted. The final version may differ from this version.

Introduction

In 2001, the hexapeptide angiotensin IV (Ang IV; Val-Tyr-Ile-His-Pro-Phe), which improves memory and learning in both rats and mice (Braszko et al., 1988; Wright et al., 1993; Wright et al., 1996; Wright et al., 1999; Lee et al., 2004; Gard et al., 2007; Braszko et al., 2008; De Bundel et al., 2009; Gard et al., 2012), was demonstrated to inhibit the membrane-bound zinc-dependent insulin-regulated aminopeptidase (EC 3.4.11.3 IRAP, oxytocinase), a member of the M1 family, which is expressed in a diversity of tissues/cells (Albiston et al., 2001; Liao et al., 2006; Saveanu and van Endert, 2012; Nikolaou et al., 2014). There has been dispute in the field as to the target that mediates the memory-enhancing effects of Ang IV as this hexapeptide has the ability to bind to other proteins (Vanderheyden, 2009; Kawas et al., 2012; Benoist et al., 2014; Wright and Harding, 2015). Nevertheless, the hypothesis that Ang IV and its analogues improve cognitive function through IRAP inhibition by altering levels of neuropeptides in the brain and/or exerting their actions by facilitating glucose uptake in neurons have attracted the most attention (Vauquelin et al., 2002; Albiston et al., 2003; Chai et al., 2004).

There is a need for improved cognitive enhancers for the treatment of Alzheimer's disease and related disorders and it is therefore not surprising that considerable efforts have been devoted to the discovery of compounds that can mimic the positive effects of Ang IV (Wolfe, 2002; Chai et al., 2008; Gard, 2008; Wright et al., 2008; Hallberg, 2009; Kawas et al., 2012; McCoy et al., 2013; Wright et al., 2015). Both potent and specific drug-like IRAP inhibitors (Borhade et al., 2014; Mountford et al., 2014), some with proven effects *in vivo* (Albiston et al., 2008; Albiston et al., 2011), and inhibitors with more peptidic character (Kobori et al., 1997; Kobori et al., 1998; Wolfe, 2002; Axen et al., 2006; Axen et al., 2007; Andersson et al., 2008; Lukaszuk et al., 2008; Hallberg, 2009; Lukaszuk et al., 2009) have been disclosed by us and others. We use an approach to discover efficient Ang IV peptidemimetics that relies on stepwise alterations of Ang IV by applying various cyclization procedures to restrict conformational

Molecular Pharmacology Fast Forward. Published on January 14, 2016 as DOI: 10.1124/mol.115.102533
This article has not been copyedited and formatted. The final version may differ from this version.

flexibility and to allow determination of the bioactive conformation of Ang IV when it binds to IRAP (Axen et al., 2006; Axen et al., 2007).

Endogenous IRAP substrates, such as the macrocyclic peptides oxytocin and vasopressin (Fig. 1), that encompass a disulphide element adjacent to the cleavage site of the ring system are known to exert favorable influences on cognition (Chai et al., 2004; Stragier et al., 2008). Our medicinal chemistry approach has taken advantage of this knowledge to develop potent macrocyclic IRAP inhibitors (Andersson et al., 2010; Andersson et al., 2011).

Previous studies have observed a correlation between the procognitive effects of Ang IV-derived peptides in rodents and their capacities to increase spine number and alter morphology (Benoist et al., 2011; McCoy et al., 2013). These data suggest that the positive impact of these peptides and peptidemimetics on cognition and dendritic spines might be attributed to a possible capacity to suppress the catalytic activity of the aminopeptidase IRAP.

We selected two macrocyclic competitive IRAP inhibitors that differ only with regard to one stereogenic center (Fig. 2), one exhibiting powerful inhibitory activity (HA08) and one that is 100-fold less potent (HA09). In this study, binding modes of the peptide inhibitor Ang IV, the macrocyclic inhibitors HA08 and HA09, and the cyclic substrate oxytocin, which is specifically hydrolyzed by IRAP, are presented by means of a computational analysis starting from the recently reported 3D structure of human IRAP (Hermans et al., 2015). We herein report that the IRAP inhibitor HA08, in contrast to the structurally similar, but less potent IRAP inhibitor, HA09, binds more favorably to the active site of IRAP and increases dendritic spine number, which provides an argument for the proposal that specific inhibition of IRAP activity accounts for the observed outcome. From this study, which includes molecular dynamics and binding free energy calculations, we envisage the structural determinants of the differences in activities experimentally reported between the different inhibitors.

Molecular Pharmacology Fast Forward. Published on January 14, 2016 as DOI: 10.1124/mol.115.102533
This article has not been copyedited and formatted. The final version may differ from this version.

Materials and Methods

Syntheses

The synthesis of HA08 and HA09 was reported previously (Andersson et al., 2010). The two macrocycles were prepared by manual solid phase peptide synthesis using the fluorenylmethoxycarbonyl chloride protection strategy followed by oxidative cyclization in solution.

Structural modeling and molecular docking

The crystal structure of human IRAP was retrieved from the protein data bank (PDB code: 4PJ6) (Hermans et al., 2015). The crystal cell is constituted by a dimer and we retained chain A for our calculations, including protein atoms and the Zn^{2+} ion. Missing side chains and hydrogens were added with the pdb2pqr tool in CHIMERA (Pettersen et al., 2004). The binding mode of Ang IV in its extended conformation was modeled by superimposing onto the crystallographic structure of Ang IV in complex with the homologous human aminopeptidase N (AP-N) (Laustsen et al., 2001; Wong et al., 2012; Hermans et al., 2015) with PDB code 4FYS (Wong et al., 2012). The initial model of the IRAP-Ang IV complex with the inverse γ-turn conformation (Ang IV-gt) of the peptide (Axen et al., 2006; Andersson et al., 2010; Andersson and Hallberg, 2012) was created by adjustment of the corresponding dihedrals at the proline residue using the PyMol Molecular Graphics System, version 1.5.0.4 (Schrödinger, LLC; NY, USA). Ligands HA08 and HA09 (Andersson et al., 2010) were modeled using Maestro, version 9.2 (Schrödinger, LLC), followed by energy minimization and a conformational search with MacroModel, version 9.9 (Schrödinger, LLC), using the OPLS-2005 (Jorgensen et al., 1996) force field and a root mean square deviation (RMSD) cut-off of 1.0Å for clustering. All the resulting ~50 conformers were docked independently with GLIDE (Halgren et al., 2004), using

Molecular Pharmacology Fast Forward. Published on January 14, 2016 as DOI: 10.1124/mol.115.102533
This article has not been copyedited and formatted. The final version may differ from this version.

XP precision on a 30Å grid centered on the Cα position of His4 in Ang IV (as docked to IRAP above). The top-10 ranked poses for each inhibitor were refined with 1 ns molecular dynamics (MD) simulations (see parameters below). Within these, we retained the binding pose that was more compatible with the binding interactions modeled for Ang IV, and this pose was subjected to further MD coupled to binding affinity calculations (see below). The models of Ang IV in the two considered conformations i.e. extended and with inverse γ-turn, were also used as starting points for binding affinity calculations. Finally, the cyclic peptide oxytocin was docked with GLIDE (same parameters as above), starting from its NMR structure (PDB code 2MGO). From the top ranked poses, we retained the binding mode where the binding interactions at the N-terminal were in most agreement to those of AngIV, and this pose was refined with 20 independent MD simulations of 10 ns length each.

MD simulations and LIE calculations

MD simulations were performed using the program Q (Marelius et al., 1998) with the OPLS-AA force field (Jorgensen et al., 1996). The parameters needed for the Zn ion and the ligands were retrieved from automatic parameterization performed with Macromodel, version 10.6 (Schrödinger, LLC), except for the partial charges of HA08 and HA09, which were parameterized based on similar compounds. Spherical boundary conditions were used, with a simulation sphere of 25Å (HA08, HA09 and Ang IV) or 30Å (oxytocin) radius centered on the same point as defined for the docking calculations. This sphere was solvated with TIP3P water molecules (Jorgensen et al., 1983) and subject to polarization and radial constraints according to the surface constrained all-atom solvent model (King and Warshel, 1989; Marelius et al., 1998) at the sphere surface, to mimic the properties of bulk water. Protein atoms outside the simulation sphere were restrained to their initial positions and only interacted with the system through bonds, angles, and torsions. The ionization states of titratable residues within 20Å of the Zn ion, as well as the residues Lys520, Lys726, Glu767, Asp773, Arg817, Glu818, Arg820,

Molecular Pharmacology Fast Forward. Published on January 14, 2016 as DOI: 10.1124/mol.115.102533
This article has not been copyedited and formatted. The final version may differ from this version.

Glu825, Arg858, Glu887, Lys890, Lys892, Glu895, Arg933 and Glu1002 were treated as ionized, while the remaining residues were modeled in their neutral form. With this setup the simulation sphere was overall neutral, thus avoiding the consideration of additional Born terms in the calculation of free energies. Non-bonded interactions were calculated explicitly up to a 10Å cutoff, except for the ligand atoms for which no cutoff was used. Beyond the cutoff, long-range electrostatics were treated with the local reaction field multipole expansion method (Lee and Warshel, 1992).

During the equilibration stage, which lasted 175 ps, the system was slowly heated to the target temperature of 310 K while the initial positional restrains on all solute heavy atoms were gradually released. In the subsequent data collection phase a step size of 1 fs was used and no restraints were applied, except for solvent bonds and angles, which were constrained using the SHAKE algorithm (Ryckaert et al., 1977). Non-bonded pair lists were updated every 25 steps while the ligand-surrounding interaction energies were sampled every 50 steps. The binding mode selected for each inhibitor was subjected to 10 independent simulations with the same conditions, but different starting velocities for binding affinity calculations (see below). Here, the production phase lasted for 2 ns, where ligand-surrounding energies were collected. In parallel, reference calculations for each ligand in water were carried out using the same protocol as in the bound state.

Binding free energies were calculated using the linear interaction energy (LIE) method (Aqvist et al., 1994; Hansson et al., 1998):

$$\Delta G_{bind}^{calc} = \alpha \Delta \langle U_{l-s}^{vdW} \rangle + \beta \Delta \langle U_{l-s}^{el} \rangle + \gamma$$

where $\Delta \langle U_{l-s}^{vdW} \rangle$ and $\Delta \langle U_{l-s}^{el} \rangle$ are the differences in the average nonpolar and polar ligand-surrounding interaction energies in the two states, i.e. free and bound. The coefficients α and β

Molecular Pharmacology Fast Forward. Published on January 14, 2016 as DOI: 10.1124/mol.115.102533
This article has not been copyedited and formatted. The final version may differ from this version.

are scaling parameters (Hansson et al., 1998; Almlof et al., 2004; Almlöf et al., 2007) for the nonpolar and polar terms, respectively. In the standard LIE model α has a value of 0.18, while β depends on the chemical nature of the ligand. The IRAP active site has a divalent zinc ion together with a cluster of carboxylates, causing very large electrostatic interaction energies with the ligands. As these interaction energies, particularly those involving the Zn^{2+} ion, will be very sensitive to the force field parameters we follow here the protocol used earlier for binding sites containing ions and treat β as a free parameter (Mishra et al., 2012). This also allows β to compensate for possible insufficient dielectric screening in the microscopic system. The final term γ is a protein-dependent constant that does not affect the relative binding free energies (Almlof et al., 2004), but is used to offset the resulting calculated energies with the experimental values. Thus, the values of β and γ in this system were parameterized to 0.19 and 7.30 kcal/mol, respectively.

Enzyme assays

Human IRAP

Solubilized, crude membranes isolated from HEK 293 cells (ATCC, Manassas, VA, USA) transfected with pCI-IRAP, were used as a source of the enzyme to analyze the efficacy of the candidate compounds to inhibit its enzymatic activity. As a negative control, membranes from vector-only transfected cells were used. The enzymatic activity of IRAP was determined by the hydrolysis of a synthetic aminopeptidase substrate L-leucine-4-methyl-7-coumarinylamide (Sigma Aldrich, St Louis, MO, USA) monitored by the release of a fluorogenic product at excitation and emission wavelengths of 380 and 430 nm, respectively. Assays were performed in 96-well plates; each well containing 1 µg of solubilized membrane protein and 25 µM substrate in a final volume of 100 µL 50 mM Tris-HCl buffer (pH 7.4). Reactions proceeded at 37°C for 30 min in a Wallac Victor3 V Multilabel counter (Perkin-Elmer, Waltham, MA, USA).

Molecular Pharmacology Fast Forward. Published on January 14, 2016 as DOI: 10.1124/mol.115.102533
This article has not been copyedited and formatted. The final version may differ from this version.

Inhibitory constants (K_i) for each of the inhibitors were determined over a range of concentrations (at 0.01 to 100 μM) and were calculated from the relationship $IC_{50} = K_i (1 + [S]/K_M)$ with GraphPad Prism 3 software (GraphPad Software Inc. San Diego, CA, USA).

Leukotriene A4 hydrolase

Recombinant human Leukotriene A4 hydrolase (LTA4H; Cayman Chemical, Ann Arbor, MI, USA) (specific activity 166 U/mg) was incubated at room temperature with 100 μM alanine-β-naphthylamide as a substrate in 50 mM Tris-HCl buffer, pH 8.0, containing 100 mM KCl with or without increasing concentrations of an inhibitor. The fluorescence was measured at excitation and emission wavelengths of 320 and 405 nm, respectively.

Aminopeptidase N

AP-N (specific activity 40 U/mg) (Sigma Aldrich) was incubated with 250 μM of substrate alanine-β-naphthylamide (Sigma Aldrich) in Tris buffered saline (50 mM Tris-HCl, 150 mM NaCl pH 7.5) at 25°C. IRAP inhibitors (1-10 μM) were added after 1 min and fluorescence was monitored at excitation and emission wavelengths of 320 and 405 nm, respectively.

Primary Hippocampal Cultures

Primary hippocampal cultures were prepared according to a previously described method (Kaech and Banker, 2006) with slight modification. In brief, pregnant Sprague Dawley rats (Charles River, Germany) were euthanized with carbon dioxide to allow the isolation of hippocampal neurons from mixed embryonic day 17 fetal rats. Hippocampi were chemically digested with 0.4 mg/mL trypsin (Sigma-Aldrich) for 10 min at 37°C, followed by mechanical dissociation with a 1 mL pipette in Hank's balanced salt solution (Invitrogen, Carlsbad, CA, USA) containing 0.5 mg/mL trypsin inhibitor (Sigma-Aldrich). Cells were seeded on 24-well

Molecular Pharmacology Fast Forward. Published on January 14, 2016 as DOI: 10.1124/mol.115.102533
This article has not been copyedited and formatted. The final version may differ from this version.

plates containing glass coverslips precoated with 50 µg/mL poly-D-lysine (MW 70,000-150,000; Sigma-Aldrich) at a density of 1×10^5 cells per well, and maintained at 37°C/5% (v/v) CO_2 in a humidified incubator. Cultures were grown in Neurobasal medium (Invitrogen) supplemented with B27 (Invitrogen), 0.5 mM GlutaMAX™ supplement (Invitrogen), and 10% (v/v) fetal bovine serum (Invitrogen) for 24 h, after which the media was replaced with serum-free media containing an additional 2% (v/v) B27. Partial media changes were performed twice a week. Hippocampal cells were grown for 13 days *in vitro* (DIV), a time when peak dendritic growth and spine formation occurs (Kaech and Banker, 2006), before the addition of varying concentrations of inhibitors on day 14, 17 and 20. Treatments were ceased at 21 DIV and were found to have no noticeable effects on cell viability, as assessed by the 3-(4,5-dimethylthiazol-2-yl)-2,5-diphenyltetrazolium bromide assay. All animal experiments were approved by the Animal Ethics Committee at Uppsala University.

Immunocytochemistry and Image Analysis

At 21 DIV, cells were fixed with 4% (w/v) paraformaldehyde containing 0.12 M sucrose. After fixation, cells were washed in phosphate buffered saline (PBS) and permeabilized with 0.2% (v/v) triton-X-100. Cells were blocked with 10% (v/v) normal donkey serum (Sigma-Aldrich) for 1 h at room temperature and incubated with either mouse anti-β III-tubulin (1:500; Sigma-Aldrich), a marker of neuronal processes, or rabbit anti-drebrin (1:500; Enzo Life Sciences, NY, USA), a marker of dendritic spines, for 90 min at room temperature. Cells were then incubated with the appropriate fluorescent-conjugated secondary antibodies (1:500; Alexa 488 and Alexa 568; Invitrogen) for 1 h at room temperature, rinsed with PBS, and mounted with MOWIOL anti-fade mounting medium (Sigma-Aldrich) containing 4',6-diamidino-2-phenylindole, dihydrochloride (DAPI; Merck Millipore, MA, USA). Images were captured using a Zeiss LSM700 inverted confocal microscope (Carl Zeiss Microscopy GmbH, Jena, Germany) with a x63 oil immersion lens. The number of total spines, stubby/mushroom-like spines and

Molecular Pharmacology Fast Forward. Published on January 14, 2016 as DOI: 10.1124/mol.115.102533
This article has not been copyedited and formatted. The final version may differ from this version.

filopodium/thin-like spines were counted on three individual basal dendrites (primary and secondary) from 10 neurons per culture (3-6 independent cultures) using Image J 1.49e software (National Institutes of Health, Bethesda, MD, USA). Selected segments were at least 50 µm away from the cell body and the numbers of spines were counted on dendritic segments spanning 50 µm. Spines were defined and quantified as previously described (Garcia et al., 2010). Two populations of spines were identified based on the morphology of the spine and intensity of drebrin staining. Spines with or without a small neck that had a small and rounded spine head ≥ 0.7 µm in diameter, exhibiting high concentrations of drebrin, were considered stubby/mushroom-like spines, while spines that were typically longer, thin, and lacked a distinguishable spine head were considered filopodium/thin-like spines. All images were captured and analyzed by a researcher blinded to the treatments. For spine functionality experiments, cells were incubated with rabbit anti-vesicular glutamate transporter 1 (vGLUT1, 1:500; Abcam, MA, USA), a marker of presynaptic glutamatergic synapses, or rabbit anti-synapsin1 (1:500; Abcam), a universal marker of presynaptic terminals. Immunostaining controls where the primary antibody was systematically removed were performed to ensure specificity of staining.

Statistical Analyses

All data were analyzed by one-way analysis of variance (ANOVA) followed by Dunnett's post hoc test using GraphPad Prism, version 5 (GraphPad Prism software Inc., La Jolla, CA, USA). A P value < 0.05 was considered statistically significant. Numerical data are represented as the mean ± S.E.M.

Molecular Pharmacology Fast Forward. Published on January 14, 2016 as DOI: 10.1124/mol.115.102533
This article has not been copyedited and formatted. The final version may differ from this version.

Results

MD simulations and LIE calculations, Ang IV, HA08 and HA09

After docking of the inhibitors HA08, HA09 and Ang IV into the IRAP active site, binding free energies (ΔG_{bind}) were calculated using MD simulations and the LIE method (Aqvist et al., 1994; Hansson et al., 1998). For Ang IV, we considered two different docking solutions corresponding to the extended and inverse γ-turn (Ang IV-gt) conformations. In optimizing the LIE β parameter we took the average of the Ang IV interaction energies (in both the bound and free states) for the two conformations, which yields an LIE model with very close agreement between calculated and observed binding free energies (Table 1). If the two Ang IV cases are instead optimized separately the predicted binding free energies are -9.7 kcal/mol for the extended conformation and -10.0 kcal/mol for Ang IV-gt. The changes in the predicted binding free energies for HA08 and HA09 are less than 0.1 kcal/mol with those models. Hence, the final calculations consistently predict HA08 to be the most potent inhibitor and also indicate that the Ang IV-gt conformation may be slightly more favorable than the extended one, although the error bars are larger for Ang IV due to the fact that it is a larger ligand.

In comparing the extended and Ang IV-gt conformations it is clear that both of these exhibit a conserved binding mode where the peptide carbonyl group of the N-terminal residue is coordinated to the Zn ion while the terminal amine is fixed by three glutamate carboxylates (Glu431, Glu487 and Glu295). However, out of six residues it is only the first two that are identical between the two conformations (Fig. 3A). Although it was observed that the inverse γ-turn slightly relaxes towards the extended Ang IV conformation during the equilibration, causing the C-terminal carboxylate group of the phenylalanine residue to move into a position similar to that of the extended conformation, the two conformations are clearly distinct. However, in comparing the electrostatic and non-polar contributions (Table 1) for the two conformations only a small difference in the unscaled electrostatic energies (~4 kcal/mol) is observed, while the

Molecular Pharmacology Fast Forward. Published on January 14, 2016 as DOI: 10.1124/mol.115.102533
This article has not been copyedited and formatted. The final version may differ from this version.

non-polar interaction energies are identical. Furthermore, it should be noted that the small calculated difference in ΔG_{bind} (~1 kcal/mol) between Ang IV and Ang IV-gt is within the errors of our calculations and it is therefore difficult to predict the most favorable conformation of the peptide.

Similar to Ang IV, the synthetic inhibitors HA08 and HA09 are also coordinated to the Zn ion and kept in position through electrostatic interactions between an amine and Glu431, Glu487 and Glu295 (Fig. 3B). The only difference between the inhibitors HA08 and HA09 is their chirality at one stereogenic centre (Andersson et al., 2010). However, this apparently small change in the structure caused an important distinction in the binding affinities to IRAP. The predicted difference in both experimental and computational binding affinities amounts to ~2.5 kcal/mol in favor of HA08. This difference essentially originates from the different conformations of the C-terminal residue. Furthermore, it can be seen from the average structures that HA08 has some key interactions that are missing for HA09. In HA08 the intramolecular conformation is clearly more favorable as the C-terminal aromatic ring interacts with the tyrosine side chain of the inhibitor and aromatic/hydrophobic packing is further stabilized by Phe550 of the enzyme (Fig. 3C). Moreover, the HA08 carboxylate group has a hydrogen bond to Tyr961 and interacts via a water molecule with the positively charged Arg929, as is the case also for Ang IV in both of its possible conformations (Fig. 3D). The C-terminal part of HA09 is generally more flexible due to its different chirality, resulting in weaker interactions with the protein.

The macrocyclic core of both HA08 and HA09 very closely mimic the conformation of Ang IV in this region and this part of the ligand is stabilized by hydrophobic interactions with Phe544 and Tyr549 (Fig. 3D). With regard to Ang IV, it was observed that its inverse γ-turn conformation relaxes somewhat during MD equilibration towards the extended conformation. This relaxation allows the C-terminal carboxylate group to move into a position similar to that of the extended conformation. As noted above, the interaction with Arg929 is clearly important for the affinity of Ang IV, but the carboxylate group is also largely solvent exposed in the substrate

Molecular Pharmacology Fast Forward. Published on January 14, 2016 as DOI: 10.1124/mol.115.102533
This article has not been copyedited and formatted. The final version may differ from this version.

cleft of IRAP. It is further noteworthy that the C-terminal aromatic ring group of HA08 can either be seen as mimicking the proline residue in the extended Ang IV or the histidine residue in Ang IV-gt, as it overlays with both of these alternatives.

IRAP selectivity for cyclic peptides

A particularity of IRAP as compared to other metallopeptidases is its unique ability to cleave cyclic peptides. We explored the binding mode of the cyclic peptide oxytocin by combining ligand docking and MD simulations. Note that, because oxytocin is a substrate of IRAP, there is no experimental data of its binding affinity, which precluded us to estimate this value computationally. Similar to the peptidic (Ang IV) and non-peptidic (HA08, HA09) inhibitors, the cyclic part of oxytocin binds deep in the catalytic domain, contributing to the coordination of the Zn ion (carbonyl of Cys^1) while maintaining strong electrostatic interactions between its free amine and Glu431, Glu487 and Glu295 (Fig. 4A). As it can be appreciated in the figure, the N-terminal fragment (Cys^1-Tyr^2) and the disulfide bridge of oxytocin nicely overlay with the corresponding fragments of HA08, supporting the design of this disulfide cyclized inhibitors (Andersson et al., 2010). The bioactive conformation of the cyclic fragment of oxytocin is particularly favored by the particular conformation of the GAMEN loop in IRAP. This observation, which was already hypothesized on the basis of the two recent crystal structures of IRAP (Hermans et al., 2015; Mpakali et al., 2015) is here further supported by the results of our MD simulations, with backbone RMSD values as low as 1.56 ± 0.2 Å for the cyclic fragment (Cys^1-Cys^6) of oxytocin and of 0.93 ± 0.1 Å for the GAMEN loop. The optimal complementarity between oxytocin and the GAMEN loop of IRAP is in stark contrast with the conformation of the same GAMEN loop found in the closest related metallopeptidases ERAP1 and ERAP2, (see Fig. 4B). Thus, our results reinforce the hypothesis that the specificity of IRAP for the cyclic peptides is, at least in part, due to the particular configuration of its GAMEN loop (Hermans et al., 2015; Mpakali et al., 2015).

Molecular Pharmacology Fast Forward. Published on January 14, 2016 as DOI: 10.1124/mol.115.102533
This article has not been copyedited and formatted. The final version may differ from this version.

Biochemical characterization of HA08 and HA09

IRAP: Kinetic analysis of the inhibition of IRAP revealed that both HA08 and HA09 are competitive inhibitors (data not shown). The macrocycle HA08 exhibited an IC_{50} value of 8.6 nM (8.24 and 9.04 nM) and HA09 an IC_{50} value of 0.71 μM (0.68 and 0.74 μM). Hence, HA08 is a 100-fold more powerful IRAP inhibitor than HA09. Previously, the Ki values for HA08 and HA09, applying a related enzymatic assay with recombinant human IRAP, were determined to be 3.3 nM and 0.242 μM, respectively (Andersson et al., 2010). **AP-N** and **LTA4H:** Regarding selectivity we found that both of the macrocyclic compounds exhibited much lower affinities for the structurally related enzymes AP-N and LTA4H. Thus, at a concentration of 10 μM for HA08, an inhibition of 36% (35% and 38%) of AP-N was encountered while only 1% (0% and 2%) inhibition was observed at the same concentration with HA09. Both HA08 and HA09 were very poor inhibitors of LTA4H, showing < 2% inhibition at 10 μM. The percent inhibition was benchmarked against 100 μM bestatin.

Effect of HA08 and HA09 on spine morphology and density

The specific inhibition of IRAP activity has previously been shown to enhance memory in naïve rats (Albiston et al., 2008). Enhanced cognitive performance has been linked to the augmentation of synaptic connectivity, which includes changes in the number and morphology of dendritic spines (Leuner et al., 2003; McCoy, 2010; Benoist et al., 2011). In order to investigate the effect of HA08 and HA09 on spine development, and their potential cognitive-enhancing effect, we used immunofluorescence to analyze spine formation in hippocampal cultures. At 21 DIV, untreated hippocampal neurons developed numerous spines (Fig. 5A), which included stubby/mushroom-like spines, a morphology associated with mature spines

Molecular Pharmacology Fast Forward. Published on January 14, 2016 as DOI: 10.1124/mol.115.102533
This article has not been copyedited and formatted. The final version may differ from this version.

(Hayashi and Shirao, 1999), and filopodium/thin-like spines, a morphology associated with immature spines (Fig. 5B) (Ziv and Smith, 1996).

Immunocytochemical staining following exposure of cells to varying concentrations of HA08 at 14, 17 and 20 DIV revealed an increase in the number of dendritic spines, with a marked increase in spine density observed at 0.1 and 1 μM (Fig. 6A). Following quantification, a significant increase in total spine density was observed at 0.01 (mean spine number = 15.2), 0.1 (mean spine number = 15.5), and 1 μM (mean spine number = 17.8), with HA08 inducing a 12.7 ($P<0.05$), 14.4 ($P<0.05$) and 30.1% ($P< 0.001$) increase in total spine number, respectively, when compared with the vehicle control (mean spine number = 13.5; Fig. 6B). In addition, an increase in the number of stubby/mushroom-like spines was observed 0.1 and 1 μM when compared with the vehicle control (0.1 μM = 21.9%, $P<0.05$; and 1 μM = 42.1%, $P<0.001$; Fig. 6C). These effects were not observed at higher or lower concentrations. No change in the number of filopodium/thin-like spines was evident (Fig. 6D). The effect of HA08 was similar to the effect seen with 24 h exposure to brain-derived neurotrophic factor (BDNF; 100 ng/mL), a known inducer of spine development in hippocampal neurons (Chapleau et al., 2008; Gu et al., 2008). Unlike HA08, the less potent IRAP inhibitor HA09 had no significant effect on spine density or morphology (Fig. 7A, B, C).

Effect of HA08 on dendritic spine functionality

An increase in spine density can result in an increase in excitatory neurotransmission, both of which are important for memory formation (Leuner et al., 2003). Given the significant increase in mushroom/stubby spines observed following exposure to 0.1 and 1 μM HA08, we next labeled cells for the presynaptic markers synapsin1 and vGLUT1. The number of stubby/mushroom-like spines staining positive for synapsin1 or vGLUT1 were counted to

Molecular Pharmacology Fast Forward. Published on January 14, 2016 as DOI: 10.1124/mol.115.102533
This article has not been copyedited and formatted. The final version may differ from this version.

determine their functional capacity (Fig. 8A, B). When compared with the vehicle control, there was no significant change in the percentage of drebrin-positive/synapsin1-positive or drebrin-positive/vGLUT1-positive spines (Fig. 8C, D), indicating that HA08 did not alter the ratio of functional synapses. However, because HA08 induced an overall increase in the number of stubby/mushroom-like spines, there was an overall increase in the number of synapsin1- and vGLUT1-positive spines compared with vehicle treated cells ($P<0.01$; Fig. 8E, F). Overall, these results suggest that HA08 may enhance excitatory input.

Molecular Pharmacology Fast Forward. Published on January 14, 2016 as DOI: 10.1124/mol.115.102533
This article has not been copyedited and formatted. The final version may differ from this version.

Discussion

IRAP is reported to be the only M1 aminopeptidase known to cleave macrocyclic rings such as those in oxytocin and vasopressin (Hermans et al., 2015). The macrocyclic HA08 that comprises a β-amino acid tyrosine residue is derived from stepwise iterative modifications of Ang IV by introduction of steric constrains by primarily 1-3 cyclizations. Proteolytic processing of peptides can lead to the formation of fragments that have very different biological activities from those of the parent peptides (Hallberg and Nyberg, 2003; Hallberg, 2015). Hence, the hypertensive octapeptide Ang II (Asp-Arg-Val-Tyr-Ile-His-Pro-Phe) is degraded to the cognitive enhancer Ang IV, which acts as an inhibitor of IRAP. The IRAP substrate oxytocin comprises a Cys-Tyr-Ile structural element in the N-terminal where Cys is enrolled in a S-S bond to a second Cys affording the large macrocyclic system of oxytocin. The Cys-Tyr bond is the primary cleavage site for IRAP. We attempted to mimic this N-terminal part of oxytocin by applying various oxidative cyclizations with cysteine and homocysteine residues in the 1-3 positions of Ang IV (Ang IV, Ki = 62 nM). However, these efforts produced only poor inhibitors *e.g*. the 1-3 cysteine analogue with a Ki of > 1000 nM and the 1-3 homocysteine analogue, with a slightly better inhibitory capacity, Ki = 303 nM (Axen et al., 2006; Axen et al., 2007; Andersson et al., 2008). Oxidative cysteine cyclizations of positions 4 and 6 of Ang IV (*i.e* His and Phe displaced), on the contrary, delivered a potent inhibitor with a Ki = 26 nM, comprising a 11-membered ring that adopts a γ-turn and by subsequent displacement of this ring system with a simplified γ-turn mimic, a phenylacetic acid derivative was afforded. Further structural optimization led to a series of potent derivatives among them the very potent IRAP inhibitor HA08 encompassing the 13-membered ring system (Andersson et al., 2010; Andersson et al., 2011).

The computational docking and MD simulations presented here predict that the macrocyclic core of HA08 and HA09, as well as the corresponding part of Ang IV, have a conserved binding mode dictated by the Zn ion and three glutamic acids. Moreover, the

Molecular Pharmacology Fast Forward. Published on January 14, 2016 as DOI: 10.1124/mol.115.102533
This article has not been copyedited and formatted. The final version may differ from this version.

cyclization strategy discussed above is supported by the bioactive conformation modeled for the cyclic peptide oxytocin. The models also predict that the chirality of the synthetic inhibitors HA08 and HA09 affect and alter both the intramolecular and the ligand-enzyme hydrophobic interactions. Here, HA08 benefits from hydrophobic packing and is stabilized by Phe550, resulting in a conformation that closely mimics the natural inhibitor Ang IV.

A reduction in spine density is an early feature of many neurodegenerative diseases (Fiala et al., 2002; Bourne and Harris, 2008; van Spronsen and Hoogenraad, 2010; Penzes et al., 2011). In particular, the specific loss of stubby/mushroom spines, which morphologically have a larger spine head and functionally have stronger synapses (Nusser et al., 1998; Matsuzaki et al., 2001; Murthy et al., 2001), is believed to have a greater impact on cognitive decline (Kasai et al., 2003). Therefore, drugs that enhance spine density have been proposed for the treatment of memory disorders (Lynch et al., 2008). IRAP inhibitors have been shown to strengthen long-term potentiation (LTP) and enhance baseline neurotransmission *in vitro* and *in vivo* (Kramar et al., 2001; Wayner et al., 2001), and changes in dendritic spine architecture, such as increased spine number or morphology, have been linked to LTP (Kasai et al., 2010) and memory (Xu et al., 2009). Given this link between synaptic density, LTP, and memory, we sought to investigate the possible relationship between IRAP inhibition and spinogenesis.

Quantification of spine density and morphology revealed that submicromolar concentrations of HA08 could significantly increase dendritic spine density and alter spine morphology in hippocampal cell cultures. Treatment with 0.1 and 1 μM HA08 for 3 days over a period of a week, resulted in spines appearing more stubby/mushroom-like, a morphology typically associated with mature spines, which are believed to have strengthened synaptic connectivity (Saneyoshi et al., 2010). In contrast, HA09 did not alter total spine density or morphology when compared with the vehicle control. Given that previous studies have shown that the procognitive activity of a molecule *in vivo* correlates well with its *in vitro* ability to alter

Molecular Pharmacology Fast Forward. Published on January 14, 2016 as DOI: 10.1124/mol.115.102533
This article has not been copyedited and formatted. The final version may differ from this version.

dendritic spine structure (Benoist et al., 2011; McCoy et al., 2013), these results suggest that HA08 may have cognitive enhancing effects.

To further investigate the effect of HA08 on dendritic spine structure, we performed functionality studies to identify their neurotransmitter signature. Immunocytochemical staining against synapsin1, a universal marker of synaptic terminals, revealed that the majority (>90%) of dendritic spines formed active synapses following 0.1 and 1 μM HA08 treatment. Dendritic spines were also vGLUT1-positive, indicating that spines were receptive to glutamatergic signaling. Interestingly, there were fewer vGLUT1-positive spines when compared with synapsin1-positive spines, suggesting that some synapses may be involved in non-glutamatergic neurotransmitter pathways, which are also known to play an important role in learning and memory processing (Jerusalinsky et al., 1997; Gong et al., 2009).

The positive effect of IRAP inhibitors on spine density and morphology may be attributed to an increase in the levels of endogenous IRAP substrates, such as oxytocin. Notably, the IRAP inhibitor Ang IV has been shown to increase levels of oxytocin in the brain *in vivo* (Beyer et al., 2010). The hippocampus is enriched with oxytocin receptors (Lee et al., 2015) and oxytocin has been shown to stimulate adult neurogenesis in the hippocampus (Leuner et al., 2012) and enhance LTP in the CA1 region (Lin et al., 2012). Therefore, the potential pro-cognitive effects of IRAP inhibitors may be mediated by increases in the levels and prolongation of activity of substrates including oxytocin. Oxytocin has recently been reported to enhance learning and memory, particularly in the novel recognition paradigm in rodents (Gard et al., 2012; Havranek et al., 2015). Although the effect of oxytocin on hippocampal dendritic spine density is not known, its effect on glucose uptake is documented. In cardiomyocytes, oxytocin has been shown to enhance glucose uptake via translocation of GLUT4 to the cell surface (Florian et al., 2010) and it is plausible that this effect may also occur in neurons. Glucose is known to facilitate memory in both humans and rodents (Manning et al., 1993; Korol and Gold,

1998; McNay et al., 2000). Interestingly, inhibitors of IRAP have also been shown to facilitate glucose uptake via the insulin-regulated glucose transporter GLUT4, which is found to colocalize with IRAP in neurons in intracellular vesicles (Fernando et al., 2008).

Overall, this study indicates that IRAP inhibition enhances spine density, a cellular process that has been closely associated with memory enhancement. However, further studies demonstrating direct cognitive enhancing effects of the IRAP inhibitor, HA08 *in vivo*, are needed.

Conclusion

There has been some dispute as to the target that mediates the memory-enhancing effects of Ang IV as this hexapeptide has the ability to bind to other proteins. The data presented herein provides support for the hypothesis that specific inhibitors of IRAP may induce the procognitive effect by altering dendritic spine density and morphology. Competitive inhibition of IRAP activity by the 13-membered macrocycle HA08 with an IC_{50} value of 8.6 nM and that mimics the N-terminal of oxytocin and vasopressin, alters the morphology of dendritic spines in primary hippocampal cultures. The number of stubby/mushroom-like spines increased, an outcome associated with improved memory. In contrast to HA08, the structurally very similar epimer HA09 with an IC_{50} value of 710 nM and which differs only with regard to its stereochemistry at one stereogenic center, did not affect spine morphology. By applying MD simulations and the LIE method, tentative modes of binding of Ang IV, HA08 and HA09 to the human IRAP can be proposed. Notably, the calculations suggest that both the extended and the γ-turn conformation of Ang IV are favorable for binding. In combination with biological assays, the capacities and differences in activities of the IRAP inhibitors Ang IV, HA08 and HA09 can be predicted by the calculations and such simulation methods, which will be valuable tools in design processes aimed at discovering novel IRAP inhibitors as potential cognitive enhancers.

Authorship Contributions:

Participated in research design: Diwakarla, Nylander, Grönbladh, Vanga, Gutiérrez-de-Terán, Ng, Sävmarker, Lundbäck, Jenmalm-Jensen, Andersson, Engen, Rosenström, Larhed, Åqvist, Chai, Hallberg

Conducted experiments: Diwakarla, Nylander, Grönbladh, Vanga, Ng, Pham, Sävmarker, Andersson

Performed data analysis: Diwakarla, Vanga, Khan, Gutiérrez-de-Terán, Ng, Åqvist

Wrote or contributed to the writing of the manuscript: Diwakarla, Vanga, Khan, Gutiérrez-de-Terán, Åqvist, Chai, Hallberg

References

Albiston AL, Diwakarla S, Fernando RN, Mountford SJ, Yeatman HR, Morgan B, Pham V, Holien JK, Parker MW, Thompson PE and Chai SY (2011) Identification and development of specific inhibitors for insulin-regulated aminopeptidase as a new class of cognitive enhancers. *Br J Pharmacol* **164**:37-47.

Albiston AL, McDowall SG, Matsacos D, Sim P, Clune E, Mustafa T, Lee J, Mendelsohn FA, Simpson RJ, Connolly LM and Chai SY (2001) Evidence that the angiotensin IV (AT(4)) receptor is the enzyme insulin- regulated aminopeptidase. *J Biol Chem* **276**:48623-48626.

Albiston AL, Morton CJ, Ng HL, Pham V, Yeatman HR, Ye S, Fernando RN, De Bundel D, Ascher DB, Mendelsohn FA, Parker MW and Chai SY (2008) Identification and characterization of a new cognitive enhancer based on inhibition of insulin-regulated aminopeptidase. *Faseb J* **22**:4209-4217.

Albiston AL, Mustafa T, McDowall SG, Mendelsohn FA, Lee J and Chai SY (2003) AT4 receptor is insulin-regulated membrane aminopeptidase: potential mechanisms of memory enhancement. *Trends Endocrinol Metab* **14**:72-77.

Almlof M, Brandsdal BO and Aqvist J (2004) Binding affinity prediction with different force fields: examination of the linear interaction energy method. *J Comput Chem* **25**:1242-1254.

Almlöf M, Carlsson J and Åqvist J (2007) Improving the Accuracy of the Linear Interaction Energy Method for Solvation Free Energies. *J Chem Theory Comput* **3**:2162-2175.

Andersson H, Demaegdt H, Johnsson A, Vauquelin G, Lindeberg G, Hallberg M, Erdelyi M, Karlen A and Hallberg A (2011) Potent macrocyclic inhibitors of insulin-regulated aminopeptidase (IRAP) by olefin ring-closing metathesis. *J Med Chem* **54**:3779-3792.

Andersson H, Demaegdt H, Vauquelin G, Lindeberg G, Karlen A and Hallberg M (2008) Ligands to the (IRAP)/AT4 receptor encompassing a 4-hydroxydiphenylmethane scaffold replacing Tyr2. *Bioorg Med Chem* **16**:6924-6935.

Andersson H, Demaegdt H, Vauquelin G, Lindeberg G, Karlen A, Hallberg M, Erdelyi M and Hallberg A (2010) Disulfide cyclized tripeptide analogues of angiotensin IV as potent and selective inhibitors of insulin-regulated aminopeptidase (IRAP). *J Med Chem* **53**:8059-8071.

Andersson H and Hallberg M (2012) Discovery of inhibitors of insulin-regulated aminopeptidase as cognitive enhancers. *Int J Hypertens* **2012**:789671.

Aqvist J, Medina C and Samuelsson JE (1994) A new method for predicting binding affinity in computer-aided drug design. *Protein Eng* **7**:385-391.

Axen A, Andersson H, Lindeberg G, Ronnholm H, Kortesmaa J, Demaegdt H, Vauquelin G, Karlen A and Hallberg M (2007) Small potent ligands to the insulin-regulated aminopeptidase (IRAP)/AT(4) receptor. *J Pept Sci* **13**:434-444.

Axen A, Lindeberg G, Demaegdt H, Vauquelin G, Karlen A and Hallberg M (2006) Cyclic insulin-regulated aminopeptidase (IRAP)/AT4 receptor ligands. *J Pept Sci* **12**:705-713.

Benoist CC, Kawas LH, Zhu M, Tyson KA, Stillmaker L, Appleyard SM, Wright JW, Wayman GA and Harding JW (2014) The procognitive and synaptogenic effects of angiotensin IV-derived peptides are dependent on activation of the hepatocyte growth factor/c-met system. *J Pharmacol Exp Ther* **351**:390-402.

Benoist CC, Wright JW, Zhu M, Appleyard SM, Wayman GA and Harding JW (2011) Facilitation of hippocampal synaptogenesis and spatial memory by C-terminal truncated Nle1-angiotensin IV analogs. *J Pharmacol Exp Ther* **339**:35-44.

Beyer CE, Dwyer JM, Platt BJ, Neal S, Luo B, Ling HP, Lin Q, Mark RJ, Rosenzweig-Lipson S and Schechter LE (2010) Angiotensin IV elevates oxytocin levels in the rat amygdala and produces anxiolytic-like activity through subsequent oxytocin receptor activation. *Psychopharmacology (Berl)* **209**:303-311.

Borhade SR, Rosenström U, Sävmarker J, Lundbäck T, Jenmalm-Jensen A, Sigmundsson K, Axelsson H, Svensson F, Konda V, Sköld C, Larhed M and Hallberg M (2014) Inhibition

of Insulin-Regulated Aminopeptidase (IRAP) by Arylsulfonamides. *ChemistryOpen* **3**:256-263.

Bourne JN and Harris KM (2008) Balancing structure and function at hippocampal dendritic spines. *Annu Rev Neurosci* **31**:47-67.

Braszko JJ, Kupryszewski G, Witczuk B and Wisniewski K (1988) Angiotensin II-(3-8)-hexapeptide affects motor activity, performance of passive avoidance and a conditioned avoidance response in rats. *Neuroscience* **27**:777-783.

Braszko JJ, Wielgat P and Walesiuk A (2008) Effect of D(3) dopamine receptors blockade on the cognitive effects of angiotensin IV in rats. *Neuropeptides* **42**:301-309.

Chai SY, Fernando R, Peck G, Ye SY, Mendelsohn FA, Jenkins TA and Albiston AL (2004) The angiotensin IV/AT4 receptor. *Cell Mol Life Sci* **61**:2728-2737.

Chai SY, Yeatman HR, Parker MW, Ascher DB, Thompson PE, Mulvey HT and Albiston AL (2008) Development of cognitive enhancers based on inhibition of insulin-regulated aminopeptidase. *BMC Neurosci* **9 Suppl 2**:S14.

Chapleau CA, Carlo ME, Larimore JL and Pozzo-Miller L (2008) The actions of BDNF on dendritic spine density and morphology in organotypic slice cultures depend on the presence of serum in culture media. *J Neurosci Methods* **169**:182-190.

De Bundel D, Smolders I, Yang R, Albiston AL, Michotte Y and Chai SY (2009) Angiotensin IV and LVV-haemorphin 7 enhance spatial working memory in rats: effects on hippocampal glucose levels and blood flow. *Neurobiol Learn Mem* **92**:19-26.

Fernando RN, Albiston AL and Chai SY (2008) The insulin-regulated aminopeptidase IRAP is colocalised with GLUT4 in the mouse hippocampus--potential role in modulation of glucose uptake in neurones? *Eur J Neurosci* **28**:588-598.

Fiala JC, Spacek J and Harris KM (2002) Dendritic spine pathology: cause or consequence of neurological disorders? *Brain Res Brain Res Rev* **39**:29-54.

Florian M, Jankowski M and Gutkowska J (2010) Oxytocin increases glucose uptake in neonatal rat cardiomyocytes. *Endocrinology* **151**:482-491.

Garcia O, Torres M, Helguera P, Coskun P and Busciglio J (2010) A role for thrombospondin-1 deficits in astrocyte-mediated spine and synaptic pathology in Down's syndrome. *PLoS One* **5**:e14200.

Gard PR (2008) Cognitive-enhancing effects of angiotensin IV. *BMC Neurosci* **9 Suppl 2**:S15.

Gard PR, Daw P, Mashhour ZS and Tran P (2007) Interactions of angiotensin IV and oxytocin on behaviour in mice. *J Renin Angiotensin Aldosterone Syst* **8**:133-138.

Gard PR, Naylor C, Ali S and Partington C (2012) Blockade of pro-cognitive effects of angiotensin IV and physostigmine in mice by oxytocin antagonism. *Eur J Pharmacol* **683**:155-160.

Gong N, Li Y, Cai GQ, Niu RF, Fang Q, Wu K, Chen Z, Lin LN, Xu L, Fei J and Xu TL (2009) GABA transporter-1 activity modulates hippocampal theta oscillation and theta burst stimulation-induced long-term potentiation. *J Neurosci* **29**:15836-15845.

Gu J, Firestein BL and Zheng JQ (2008) Microtubules in dendritic spine development. *J Neurosci* **28**:12120-12124.

Halgren TA, Murphy RB, Friesner RA, Beard HS, Frye LL, Pollard WT and Banks JL (2004) Glide: a new approach for rapid, accurate docking and scoring. 2. Enrichment factors in database screening. *J Med Chem* **47**:1750-1759.

Hallberg M (2009) Targeting the insulin-regulated aminopeptidase/AT4 receptor for cognitive disorders. *Drug News Perspect* **22**:133-139.

Hallberg M (2015) Neuropeptides: metabolism to bioactive fragments and the pharmacology of their receptors. *Med Res Rev* **35**:464-519.

Hallberg M and Nyberg F (2003) Neuropeptide conversion to bioactive fragments--an important pathway in neuromodulation. *Curr Protein Pept Sci* **4**:31-44.

Hansson T, Marelius J and Aqvist J (1998) Ligand binding affinity prediction by linear interaction energy methods. *J Comput Aided Mol Des* **12**:27-35.

Havranek T, Zatkova M, Lestanova Z, Bacova Z, Mravec B, Hodosy J, Strbak V and Bakos J (2015) Intracerebroventricular oxytocin administration in rats enhances object recognition and increases expression of neurotrophins, microtubule-associated protein 2, and synapsin I. *J Neurosci Res* **93**:893-901.

Hayashi K and Shirao T (1999) Change in the shape of dendritic spines caused by overexpression of drebrin in cultured cortical neurons. *J Neurosci* **19**:3918-3925.

Hermans SJ, Ascher DB, Hancock NC, Holien JK, Michell BJ, Chai SY, Morton CJ and Parker MW (2015) Crystal structure of human insulin-regulated aminopeptidase with specificity for cyclic peptides. *Protein Sci* **24**:190-199.

Jerusalinsky D, Kornisiuk E and Izquierdo I (1997) Cholinergic neurotransmission and synaptic plasticity concerning memory processing. *Neurochem Res* **22**:507-515.

Jorgensen WL, Chandrasekhar J, Madura JD, Impey RW and Klein ML (1983) Comparison of simple potential functions for simulating liquid water. *J Chem Phys* **79**:926-935.

Jorgensen WL, Maxwell DS and Tirado-Rives J (1996) Development and Testing of the OPLS All-Atom Force Field on Conformational Energetics and Properties of Organic Liquids. *J Am Chem Soc* **118**:11225-11236.

Kaech S and Banker G (2006) Culturing hippocampal neurons. *Nat Protoc* **1**:2406-2415.

Kasai H, Fukuda M, Watanabe S, Hayashi-Takagi A and Noguchi J (2010) Structural dynamics of dendritic spines in memory and cognition. *Trends Neurosci* **33**:121-129.

Kasai H, Matsuzaki M, Noguchi J, Yasumatsu N and Nakahara H (2003) Structure-stability-function relationships of dendritic spines. *Trends Neurosci* **26**:360-368.

Kawas LH, McCoy AT, Yamamoto BJ, Wright JW and Harding JW (2012) Development of angiotensin IV analogs as hepatocyte growth factor/Met modifiers. *J Pharmacol Exp Ther* **340**:539-548.

King G and Warshel A (1989) A surface constrained all-atom solvent model for effective simulations of polar solutions. *J Chem Phys* **91**:3647-3661.

Kobori T, Goda K, Sugimoto K, Ota T and Tomisawa K (1997) Preparation of peptide derivatives as angiotensin IV receptor agonists. *WO 97/03093 A1*.

Kobori T, Goda K, Sugimoto K, Ota T and Tomisawa K (1998) Preparation of amino acid derivatives as angiotensin IV receptor agonists. *WO 98/05624 A1*.

Korol DL and Gold PE (1998) Glucose, memory, and aging. *Am J Clin Nutr* **67**:764S-771S.

Kramar EA, Armstrong DL, Ikeda S, Wayner MJ, Harding JW and Wright JW (2001) The effects of angiotensin IV analogs on long-term potentiation within the CA1 region of the hippocampus in vitro. *Brain Res* **897**:114-121.

Laustsen PG, Vang S and Kristensen T (2001) Mutational analysis of the active site of human insulin-regulated aminopeptidase. *Eur J Biochem* **268**:98-104.

Lee FS and Warshel A (1992) A local reaction field method for fast evaluation of long-range electrostatic interactions in molecular simulations. *J Chem Phys* **97**:3100-3107.

Lee J, Albiston AL, Allen AM, Mendelsohn FA, Ping SE, Barrett GL, Murphy M, Morris MJ, McDowall SG and Chai SY (2004) Effect of I.C.V. injection of AT4 receptor ligands, NLE1-angiotensin IV and LVV-hemorphin 7, on spatial learning in rats. *Neuroscience* **124**:341-349.

Lee SY, Park SH, Chung C, Kim JJ, Choi SY and Han JS (2015) Oxytocin Protects Hippocampal Memory and Plasticity from Uncontrollable Stress. *Sci Rep* **5**:18540.

Leuner B, Caponiti JM and Gould E (2012) Oxytocin stimulates adult neurogenesis even under conditions of stress and elevated glucocorticoids. *Hippocampus* **22**:861-868.

Leuner B, Falduto J and Shors TJ (2003) Associative memory formation increases the observation of dendritic spines in the hippocampus. *J Neurosci* **23**:659-665.

Liao H, Keller SR and Castle JD (2006) Insulin-regulated aminopeptidase marks an antigen-stimulated recycling compartment in mast cells. *Traffic* **7**:155-167.

Lin YT, Huang CC and Hsu KS (2012) Oxytocin promotes long-term potentiation by enhancing epidermal growth factor receptor-mediated local translation of protein kinase Mzeta. *J Neurosci* **32**:15476-15488.

Lukaszuk A, Demaegdt H, Feytens D, Vanderheyden P, Vauquelin G and Tourwe D (2009) The replacement of His(4) in angiotensin IV by conformationally constrained residues provides highly potent and selective analogues. *J Med Chem* **52**:5612-5618.

Lukaszuk A, Demaegdt H, Szemenyei E, Toth G, Tymecka D, Misicka A, Karoyan P, Vanderheyden P, Vauquelin G and Tourwe D (2008) Beta-homo-amino acid scan of angiotensin IV. *J Med Chem* **51**:2291-2296.

Lynch G, Rex CS, Chen LY and Gall CM (2008) The substrates of memory: defects, treatments, and enhancement. *Eur J Pharmacol* **585**:2-13.

Manning CA, Ragozzino ME and Gold PE (1993) Glucose enhancement of memory in patients with probable senile dementia of the Alzheimer's type. *Neurobiol Aging* **14**:523-528.

Marelius J, Kolmodin K, Feierberg I and Aqvist J (1998) Q: a molecular dynamics program for free energy calculations and empirical valence bond simulations in biomolecular systems. *J Mol Graph Model* **16**:213-225, 261.

Matsuzaki M, Ellis-Davies GC, Nemoto T, Miyashita Y, Iino M and Kasai H (2001) Dendritic spine geometry is critical for AMPA receptor expression in hippocampal CA1 pyramidal neurons. *Nat Neurosci* **4**:1086-1092.

McCoy A (2010) Pharmacokinetic Characterization of Angiotensin IV Analogs with Therapeutic Potential for Cancer and Dementia, in *Thesis from Department of Veterinary and Comparative Anatomy, Pharmacology, and Physiology* pp 1-139, Washington State University, Washington DC.

McCoy AT, Benoist CC, Wright JW, Kawas LH, Bule-Ghogare JM, Zhu M, Appleyard SM, Wayman GA and Harding JW (2013) Evaluation of metabolically stabilized angiotensin IV analogs as procognitive/antidementia agents. *J Pharmacol Exp Ther* **344**:141-154.

McNay EC, Fries TM and Gold PE (2000) Decreases in rat extracellular hippocampal glucose concentration associated with cognitive demand during a spatial task. *Proc Natl Acad Sci U S A* **97**:2881-2885.

Mishra SK, Sund J, Aqvist J and Koca J (2012) Computational prediction of monosaccharide binding free energies to lectins with linear interaction energy models. *J Comput Chem* **33**:2340-2350.

Mountford SJ, Albiston AL, Charman WN, Ng L, Holien JK, Parker MW, Nicolazzo JA, Thompson PE and Chai SY (2014) Synthesis, structure-activity relationships and brain uptake of a novel series of benzopyran inhibitors of insulin-regulated aminopeptidase. *J Med Chem* **57**:1368-1377.

Mpakali A, Saridakis E, Harlos K, Zhao Y, Papakyriakou A, Kokkala P, Georgiadis D and Stratikos E (2015) Crystal Structure of Insulin-Regulated Aminopeptidase with Bound Substrate Analogue Provides Insight on Antigenic Epitope Precursor Recognition and Processing. *J Immunol* **195**:2842-2851.

Murthy VN, Schikorski T, Stevens CF and Zhu Y (2001) Inactivity produces increases in neurotransmitter release and synapse size. *Neuron* **32**:673-682.

Nikolaou A, Stijlemans B, Laoui D, Schouppe E, Tran HT, Tourwe D, Chai SY, Vanderheyden PM and Van Ginderachter JA (2014) Presence and regulation of insulin-regulated aminopeptidase in mouse macrophages. *J Renin Angiotensin Aldosterone Syst* **15**:466-479.

Nusser Z, Lujan R, Laube G, Roberts JD, Molnar E and Somogyi P (1998) Cell type and pathway dependence of synaptic AMPA receptor number and variability in the hippocampus. *Neuron* **21**:545-559.

Penzes P, Cahill ME, Jones KA, VanLeeuwen JE and Woolfrey KM (2011) Dendritic spine pathology in neuropsychiatric disorders. *Nat Neurosci* **14**:285-293.

Pettersen EF, Goddard TD, Huang CC, Couch GS, Greenblatt DM, Meng EC and Ferrin TE (2004) UCSF Chimera--a visualization system for exploratory research and analysis. *J Comput Chem* **25**:1605-1612.

Ryckaert J-P, Ciccotti G and Berendsen HJC (1977) Numerical integration of the cartesian equations of motion of a system with constraints: molecular dynamics of n-alkanes. *J Comput Phys* **23**:327-341.

Saneyoshi T, Fortin DA and Soderling TR (2010) Regulation of spine and synapse formation by activity-dependent intracellular signaling pathways. *Curr Opin Neurobiol* **20**:108-115.

Saveanu L and van Endert P (2012) The role of insulin-regulated aminopeptidase in MHC class I antigen presentation. *Front Immunol* **3**:57.

Stragier B, De Bundel D, Sarre S, Smolders I, Vauquelin G, Dupont A, Michotte Y and Vanderheyden P (2008) Involvement of insulin-regulated aminopeptidase in the effects of the renin-angiotensin fragment angiotensin IV: a review. *Heart Fail Rev* **13**:321-337.

van Spronsen M and Hoogenraad CC (2010) Synapse pathology in psychiatric and neurologic disease. *Curr Neurol Neurosci Rep* **10**:207-214.

Vanderheyden PM (2009) From angiotensin IV binding site to AT4 receptor. *Mol Cell Endocrinol* **302**:159-166.

Vauquelin G, Michotte Y, Smolders I, Sarre S, Ebinger G, Dupont A and Vanderheyden P (2002) Cellular targets for angiotensin II fragments: pharmacological and molecular evidence. *J Renin Angiotensin Aldosterone Syst* **3**:195-204.

Wayner MJ, Armstrong DL, Phelix CF, Wright JW and Harding JW (2001) Angiotensin IV enhances LTP in rat dentate gyrus in vivo. *Peptides* **22**:1403-1414.

Wolfe MS (2002) Therapeutic strategies for Alzheimer's disease. *Nat Rev Drug Discov* **1**:859-866.

Wong AH, Zhou D and Rini JM (2012) The X-ray crystal structure of human aminopeptidase N reveals a novel dimer and the basis for peptide processing. *J Biol Chem* **287**:36804-36813.

Wright JW, Clemens JA, Panetta JA, Smalstig EB, Weatherly LA, Kramar EA, Pederson ES, Mungall BH and Harding JW (1996) Effects of LY231617 and angiotensin IV on ischemia-induced deficits in circular water maze and passive avoidance performance in rats. *Brain Res* **717**:1-11.

Wright JW and Harding JW (2015) The Brain Hepatocyte Growth Factor/c-Met Receptor System: A New Target for the Treatment of Alzheimer's Disease. *J Alzheimers Dis* **45**:985-1000.

Wright JW, Kawas LH and Harding JW (2015) The development of small molecule angiotensin IV analogs to treat Alzheimer's and Parkinson's diseases. *Prog Neurobiol* **125**:26-46.

Wright JW, Miller-Wing AV, Shaffer MJ, Higginson C, Wright DE, Hanesworth JM and Harding JW (1993) Angiotensin II(3-8) (ANG IV) hippocampal binding: potential role in the facilitation of memory. *Brain Res Bull* **32**:497-502.

Wright JW, Stubley L, Pederson ES, Kramar EA, Hanesworth JM and Harding JW (1999) Contributions of the brain angiotensin IV-AT4 receptor subtype system to spatial learning. *J Neurosci* **19**:3952-3961.

Wright JW, Yamamoto BJ and Harding JW (2008) Angiotensin receptor subtype mediated physiologies and behaviors: new discoveries and clinical targets. *Prog Neurobiol* **84**:157-181.

Xu T, Yu X, Perlik AJ, Tobin WF, Zweig JA, Tennant K, Jones T and Zuo Y (2009) Rapid formation and selective stabilization of synapses for enduring motor memories. *Nature* **462**:915-919.

Ziv NE and Smith SJ (1996) Evidence for a role of dendritic filopodia in synaptogenesis and spine formation. *Neuron* **17**:91-102.

Molecular Pharmacology Fast Forward. Published on January 14, 2016 as DOI: 10.1124/mol.115.102533
This article has not been copyedited and formatted. The final version may differ from this version.

Footnote

This work was supported by grants from the Swedish Research Council to the Department of Pharmaceutical Biosciences, the Department of Medicinal Chemistry and the Department of Cell and Molecular Biology, and from the Kjell and Märta Beijer Foundation to the Department of Pharmaceutical Biosciences and to the Department of Medicinal Chemistry at Uppsala University.

Molecular Pharmacology Fast Forward. Published on January 14, 2016 as DOI: 10.1124/mol.115.102533
This article has not been copyedited and formatted. The final version may differ from this version.

Figure Legends

Figure 1: The macrocyclic peptides oxytocin and vasopressin.

Figure 2: The macrocyclic IRAP inhibitors HA08 and HA09.

Figure 3. Superimposed average structures from MD simulations.
(A) The extended Ang IV (cyan) and Ang IV-gt (yellow) conformations. (B) The synthetic inhibitors HA08 (magenta) and HA09 (green). (C) Close-up of the hydrophobic packing of HA08 and HA09. (D) HA08 (magenta), and Ang IV-gt (yellow). The key residues contributing to binding are shown. The zinc ion is represented as a grey sphere.

Figure 4. Binding mode of oxytocin in IRAP.
(A) Superposition of oxytocin (green sticks) with the cyclic inhibitor HA08 (magenta), extracted from representative snapshots from the respective MD simulations. Note that the conformation of the GAMEN loop is invariable in the two cases (red, oxytocin-bound structure; gray, HA08 bound structure). (B) The GAMEN loop in IRAP (PDB code 4PJ6, cyan; representative snapshot from MD simulations with oxytocin, red), is compared with the GAMEN loop of ERAP1 (PDB code 2YDO, blue) and ERAP2 (4JBS, yellow).

Figure 5: Dendritic spine development in primary cultures of hippocampal cells.
(A) At 21 div, hippocampal cells were fixed and immunostained against β-III tubulin (1:500, green) and drebrin (1:500, red) to visualize neuronal processes and dendritic spines, respectively. Nuclei were counterstained with DAPI (blue). (B) Asterisks indicate different spine morphologies (white=stubby/mushroom-like spines; yellow=filopodium/thin-like spines). Scale bar = 20 µm.

Molecular Pharmacology Fast Forward. Published on January 14, 2016 as DOI: 10.1124/mol.115.102533
This article has not been copyedited and formatted. The final version may differ from this version.

Figure 6: Effect of HA08 on dendritic spine number and morphology.

Cultures were exposed to varying concentrations of HA08 at 14, 17 and 20 *div*. Spine number and morphology were assessed along 50 µm of dendrite in 10 neurons (3 dendrites per neuron; n = 5 independent cultures). (A) Representative images of dendritic segments depicting changes in spine density. (B) Dose-response of the percentage change in total spine number following HA08 exposure compared with the vehicle control (0.1% DMSO). (C) Dose-response of the percentage change in stubby/mushroom-like spine number following HA08 exposure compared with the vehicle control. (D) No change in filopodium/thin-like spine number was observed following HA08 exposure compared with the vehicle control. Brain-derived neurotrophic factor (100 ng/mL) was included as a positive control. Data were analyzed by one-way ANOVA followed by Dunnett's test. All data are expressed as the mean ± S.E.M. *P<0.05, ***P<0.001 compared with vehicle. Scale bar = 10 µm.

Figure 7: Effect of HA09 on dendritic spine number and morphology

Cultures were exposed to varying concentrations of HA09 at 14, 17 and 20 *div*. Spine number and morphology were assessed along 50 µm of dendrite in 10 neurons (3 dendrites per neuron; n = 5 independent cultures). No change in (A) total spine number, (B) stubby/mushroom-like spine number, or (C) filopodium/thin-like spine number was observed following HA09 exposure when compared with the vehicle control. Brain-derived neurotrophic factor (100 ng/mL) was included as a positive control. Data were analyzed by one-way ANOVA followed by Dunnett's test. All data are expressed as the mean ± S.E.M. ***P<0.001 compared with vehicle.

Figure 8. Effect of HA08 on dendritic spine function.

Molecular Pharmacology Fast Forward. Published on January 14, 2016 as DOI: 10.1124/mol.115.102533
This article has not been copyedited and formatted. The final version may differ from this version.

Cultures were exposed to 0.1 μM and 1 μM HA08 at 14, 17 and 20 *div*. Spines were labeled for synapsin1 and vGLUT1, and the numbers of spines were counted on a 50 μm length of dendrite. The functionality of spines was assessed along 50 μm of dendrite in 10 neurons (3 dendrites per neuron; n = 3 independent cultures). (A) Representative image of a dendritic segment indicating drebrin-positive (red) and synapsin1-positive (green) spines. (B) Representative image of a dendritic segment indicating drebrin-positive (red) and vGLUT1-positive (green) spines. (C) With respect to stubby/mushroom-like spines, there were no differences in the proportion of synapsin1-positive spines or (D) v-GLUT1-positve spines when compared to vehicle. Overall, there was a significant increase in the overall number of (E) synapsin1-positive and (F) vGLUT1-positive spines compared with vehicle. Data were analyzed by one-way ANOVA followed by Dunnett's test. All data are expressed as the mean ± S.E.M. **P<0.01 compared with vehicle. Scale bar = 10 μm.

Molecular Pharmacology Fast Forward. Published on January 14, 2016 as DOI: 10.1124/mol.115.102533
This article has not been copyedited and formatted. The final version may differ from this version.

Table 1. Experimental and calculated binding free energies (in kcal/mol) for the IRAP inhibitors.[a]

Ligand	Free		Bound		Enzyme	ΔG_{bind}^{obs}	ΔG_{bind}^{calc}
	$\langle U_{l-s}^{el} \rangle$	$\langle U_{l-s}^{vdW} \rangle$	$\langle U_{l-s}^{el} \rangle$	$\langle U_{l-s}^{vdW} \rangle$	$K_i \pm$ SD (nM)	(kcal/mol)	(kcal/mol)
HA08	-321.9 ± 2.5	-23.9 ± 0.2	-401.9 ± 0.7	-43.1 ± 0.2	3.3 ± 0.8	-11.6 ± 0.1	-11.6 ± 0.5
Ang IV	-357.8 ± 1.6	-37.9 ± 0.2	-417.9 ± 5.1	-66.6 ± 0.7	62.4 ± 17.5	-9.8 ± 0.2	-9.5 ± 1.0
Ang IV (γ-turn)	-346.0 ± 2.3	-35.9 ± 0.3	-409.6 ± 4.4	-64.6 ± 0.8	62.4 ± 17.5	-9.8 ± 0.2	-10.2 ± 1.0
HA09	-329.3 ± 1.4	-25.1 ± 0.1	-396.8 ± 1.3	-42.9 ± 0.4	242.0 ± 72.0	-9.0 ± 0.2	-8.9 ± 0.4

[a]Calculated binding free energies are obtained with an optimized LIE model, with β=0.19 and γ=7.3 kcal/mol. Error bars denote S.E.M for replicate simulations.

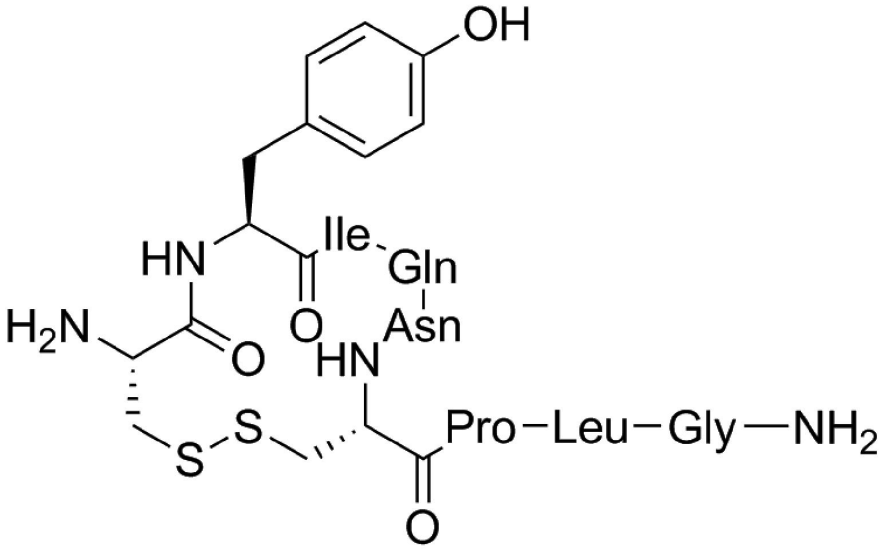

oxytocin

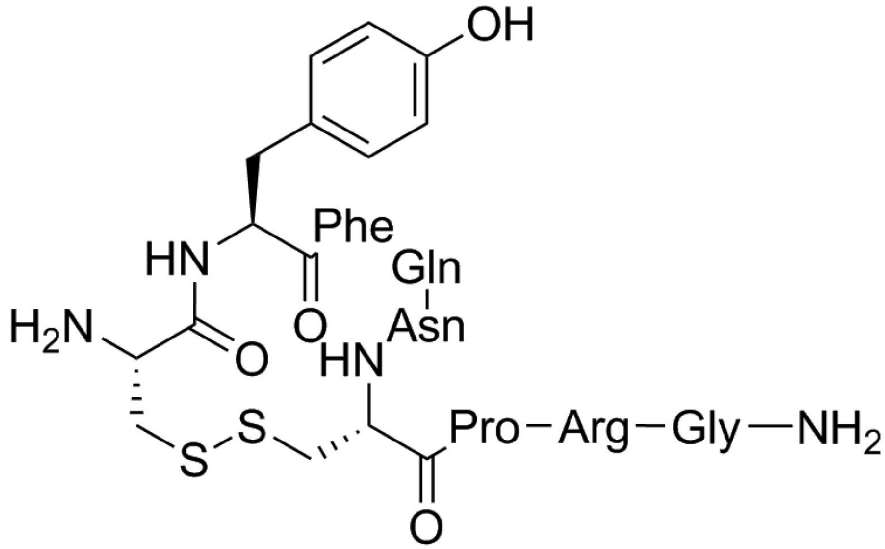

vasopressin

Figure 1

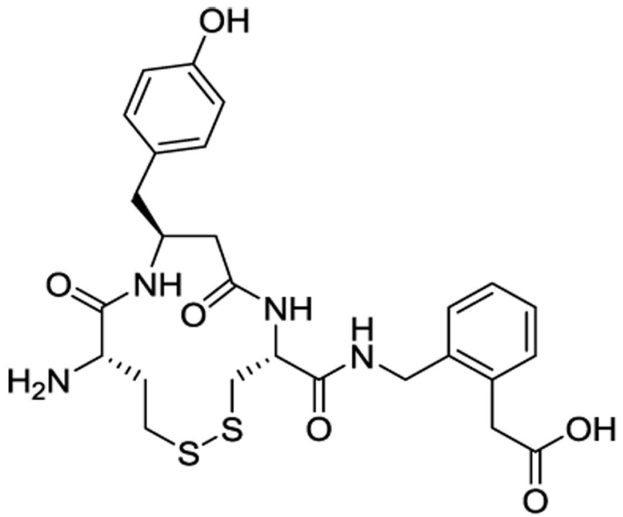

HA08

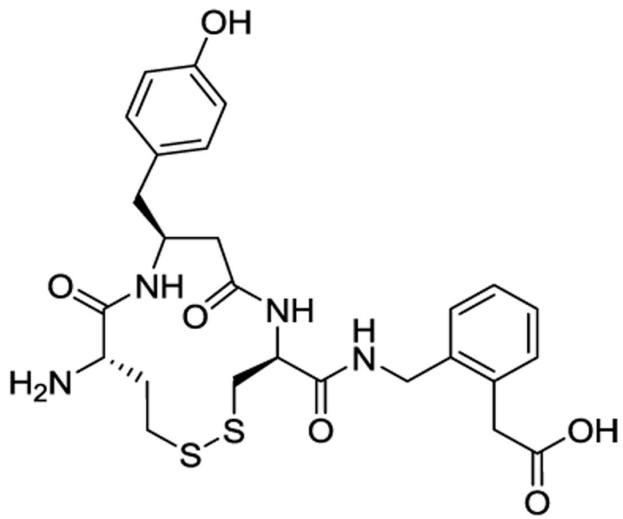

HA09

Figure 2

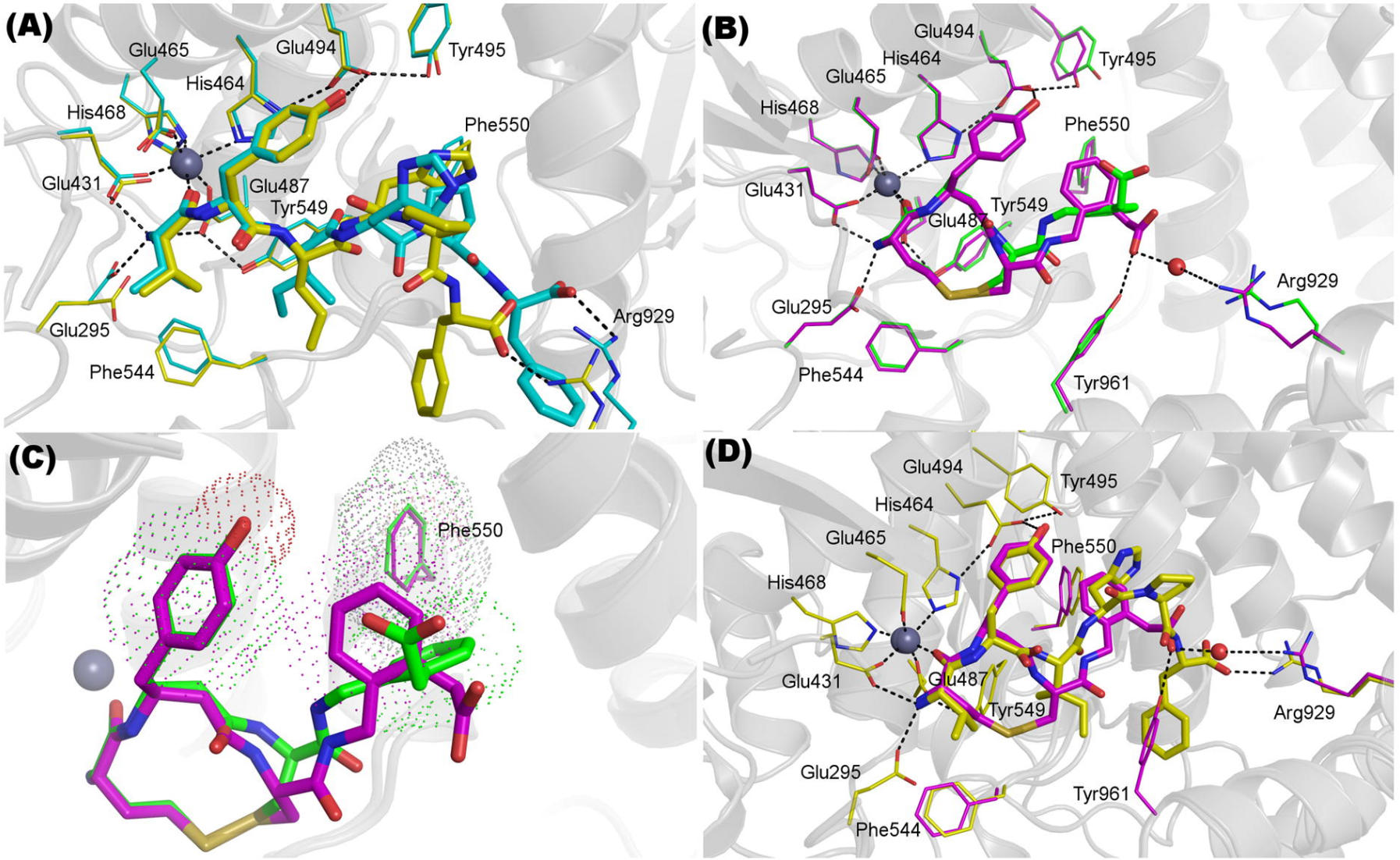
(A)
Glu465
Glu494
Tyr495
His464
His468
Phe550
Glu431
Glu487
Tyr549
Glu295
Arg929
Phe544
(B)
Glu494
His464
Tyr495
Glu465
His468
Phe550
Glu431
Tyr549
Glu487
Arg929
Glu295
Phe544
Tyr961
(C)
Phe550
(D)
Glu494
Tyr495
His464
Glu465
Phe550
His468
Glu431
Glu487
Tyr549
Arg929
Glu295
Tyr961
Phe544

Figure 3

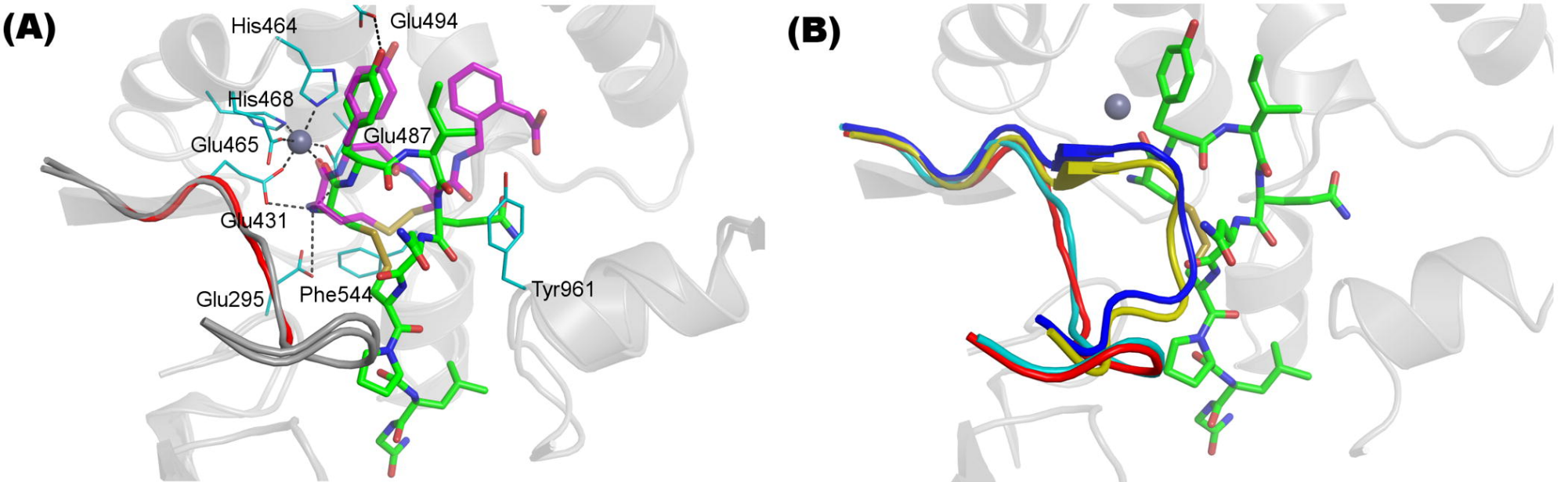
(A)
His464
Glu494
His468
Glu465
Glu487
Glu431
Glu295
Phe544
Tyr961
(B)

Figure 4

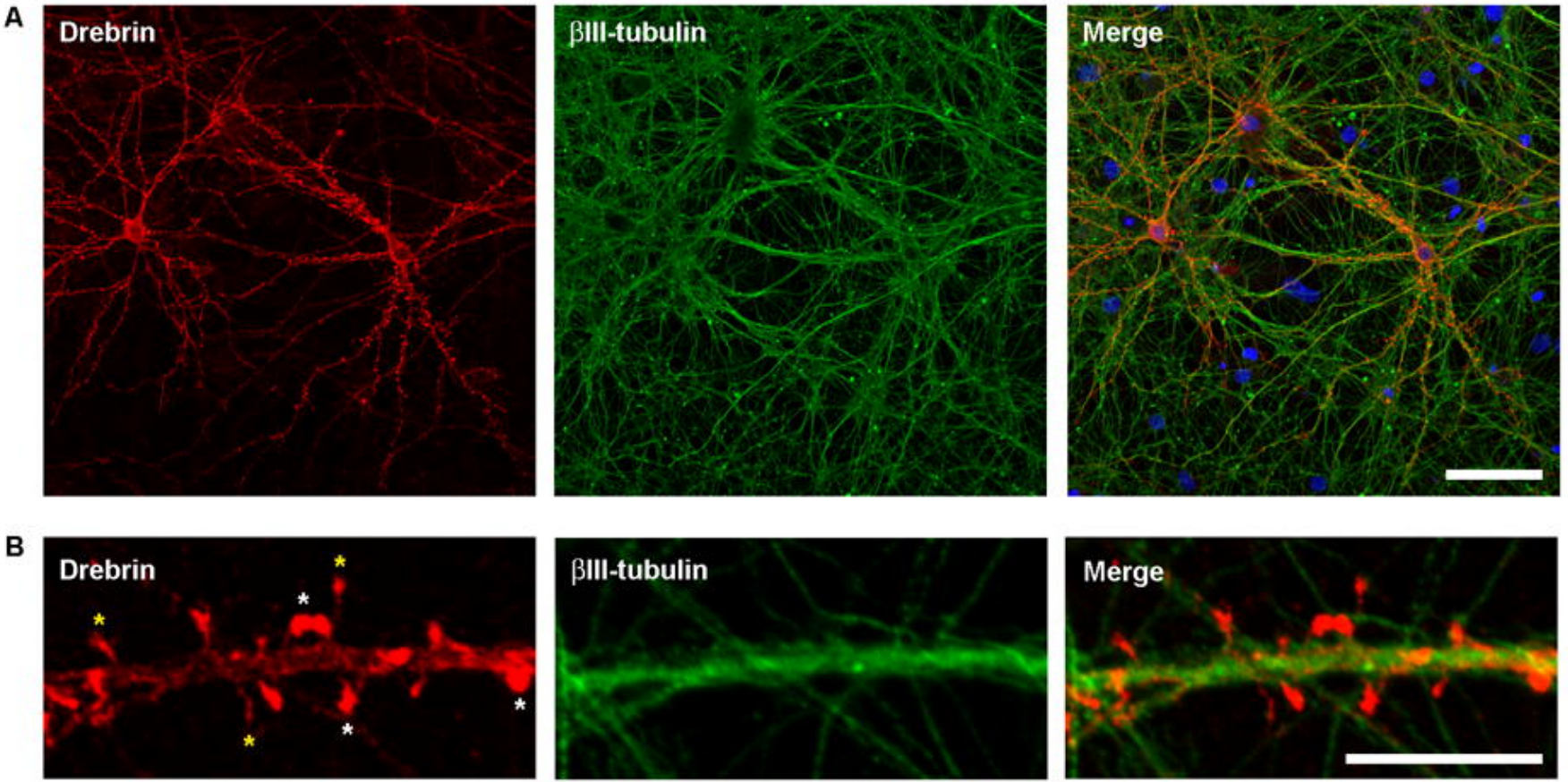

Figure 5

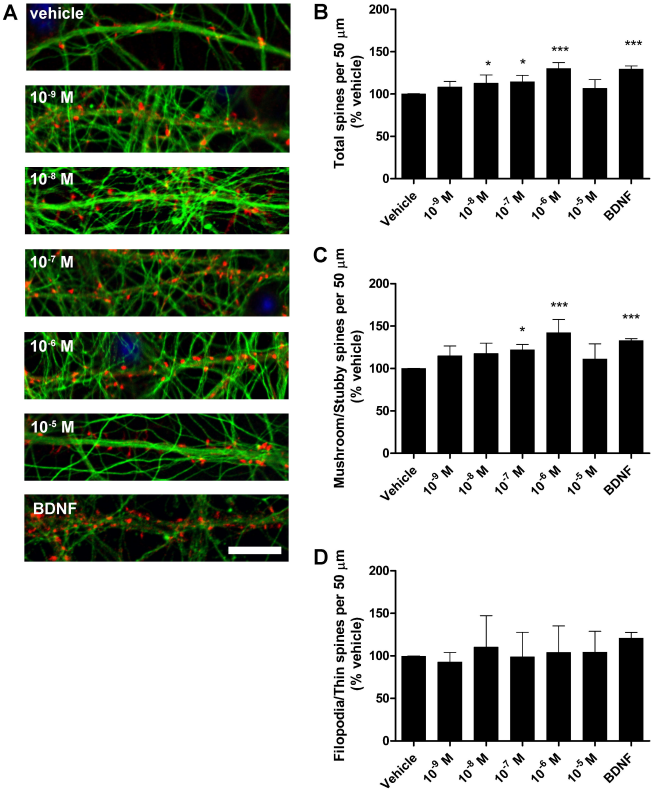
A
vehicle
10-9 M
10-8 M
10-7 M
10-6 M
10-5 M
BDNF
B
Total spines per 50 µm (% vehicle)
200
150
100
50
0
*
*
***
***
Vehicle
10-9 M
10-8 M
10-7 M
10-6 M
10-5 M
BDNF
C
Mushroom/Stubby spines per 50 µm (% vehicle)
200
150
100
50
0
*
***
***
Vehicle
10-9 M
10-8 M
10-7 M
10-6 M
10-5 M
BDNF
D
Filopodia/Thin spines per 50 µm (% vehicle)
200
150
100
50
0
Vehicle
10-9 M
10-8 M
10-7 M
10-6 M
10-5 M
BDNF

Figure 6

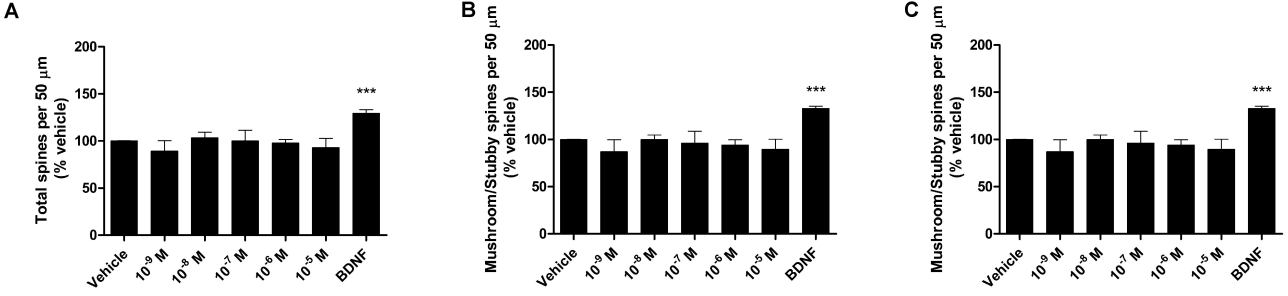
A
Total spines per 50 μm
(% vehicle)
200
150
100
50
0
***
Vehicle
10-9 M
10-8 M
10-7 M
10-6 M
10-5 M
BDNF
B
Mushroom/Stubby spines per 50 μm
(% vehicle)
200
150
100
50
0
***
Vehicle
10-9 M
10-8 M
10-7 M
10-6 M
10-5 M
BDNF
C
Mushroom/Stubby spines per 50 μm
(% vehicle)
200
150
100
50
0
***
Vehicle
10-9 M
10-8 M
10-7 M
10-6 M
10-5 M
BDNF

Figure 7

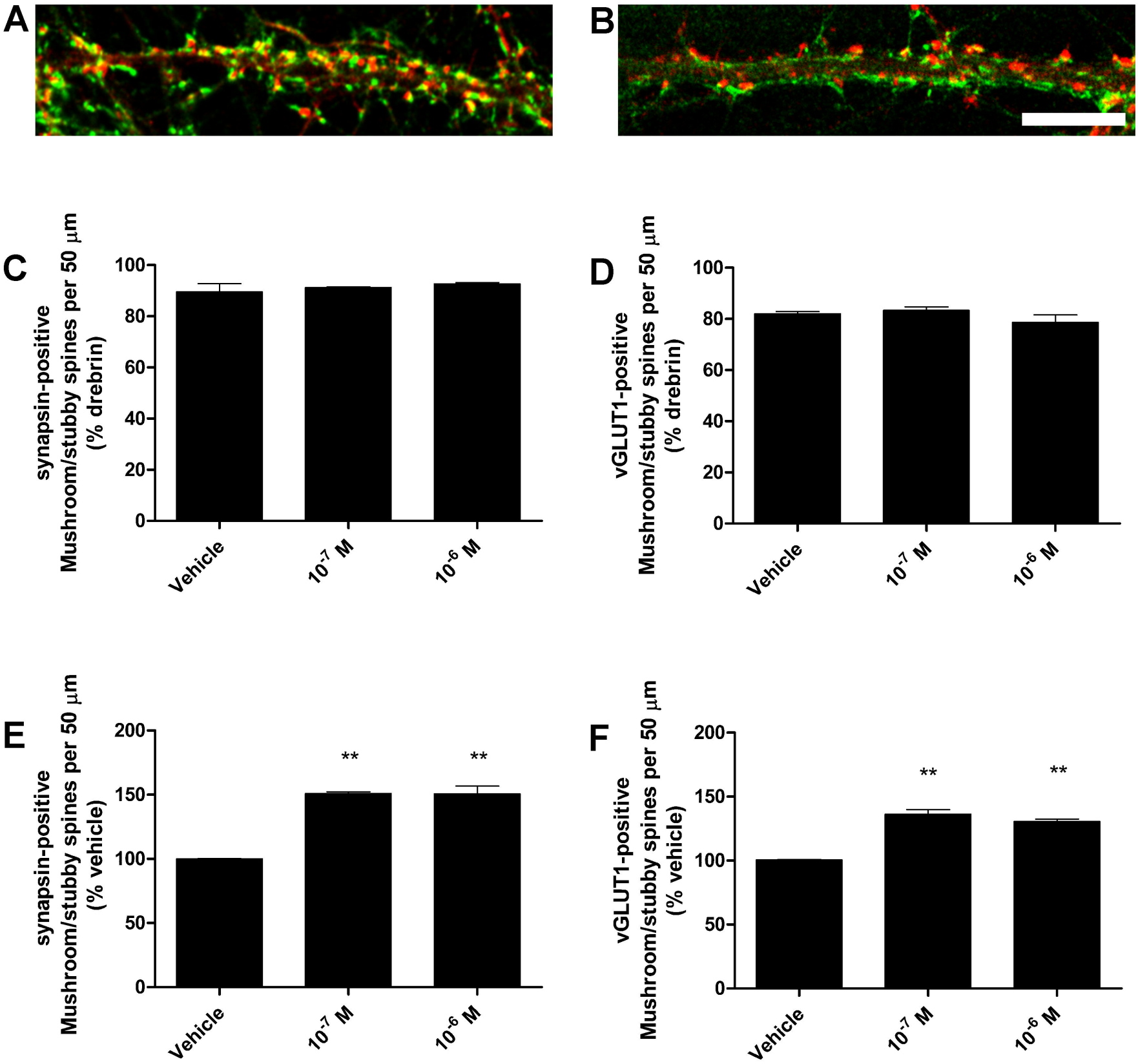
A
B
C
synapsin-positive
Mushroom/stubby spines per 50 μm
(% drebrin)
100
80
60
40
20
0
Vehicle
10-7 M
10-6 M
D
vGLUT1-positive
Mushroom/stubby spines per 50 μm
(% drebrin)
100
80
60
40
20
0
Vehicle
10-7 M
10-6 M
E
synapsin-positive
Mushroom/stubby spines per 50 μm
(% vehicle)
200
150
100
50
0
**
**
Vehicle
10-7 M
10-6 M
F
vGLUT1-positive
Mushroom/stubby spines per 50 μm
(% vehicle)
200
150
100
50
0
**
**
Vehicle
10-7 M
10-6 M

Figure 8